

SANDIA REPORT

SAND96-1168 • UC-705

Unlimited Release

Printed February 1997

Algorithm for Image Registration and Clutter and Jitter Noise Reduction

K.L. Brower

Prepared by
Sandia National Laboratories
Albuquerque, New Mexico 87185 and Livermore, California 94550
for the United States Department of Energy
under Contract DE-AC04-94AL85000

Approved for public release; distribution is unlimited.

Issued by Sandia National Laboratories, operated for the United States Department of Energy by Sandia Corporation.

NOTICE: This report was prepared as an account of work sponsored by an agency of the United States Government. Neither the United States Government nor any agency thereof, nor any of their employees, nor any of their contractors, subcontractors, or their employees, makes any warranty, express or implied, or assumes any legal liability or responsibility for the accuracy, completeness, or usefulness of any information, apparatus, product, or process disclosed, or represents that its use would not infringe privately owned rights. Reference herein to any specific commercial product, process, or service by trade name, trademark, manufacturer, or otherwise, does not necessarily constitute or imply its endorsement, recommendation, or favoring by the United States Government, any agency thereof or any of their contractors or subcontractors. The views and opinions expressed herein do not necessarily state or reflect those of the United States Government, any agency thereof or any of their contractors.

Printed in the United States of America. This report has been reproduced directly from the best available copy.

Available to DOE and DOE contractors from
Office of Scientific and Technical Information
PO Box 62
Oak Ridge, TN 37831

Prices available from (615) 576-8401, FTS 626-8401

Available to the public from
National Technical Information Service
US Department of Commerce
5285 Port Royal Rd
Springfield, VA 22161

NTIS price codes
Printed copy: A08
Microfiche copy: A01

Algorithm for Image Registration and Clutter and Jitter Noise Reduction

K. L. Brower

Mission Analysis and Simulation

Sandia National Laboratories

P.O. Box 5800

Albuquerque, NM 87185-0977

Abstract

This paper presents an analytical, computational method whereby two-dimensional images of an optical source represented in terms of a set of detector array signals can be registered with respect to a reference set of detector array signals. The detector image is recovered from the detector array signals and represented over a local region by a fourth order, two-dimensional Taylor series. This local detector image can then be registered by a general linear transformation with respect to a reference detector image. The detector signal in the reference frame is reconstructed by integrating this detector image over the respective reference pixel. For cases in which the general linear transformation is uncertain by up to plus-or-minus two pixels, the general linear transformation can be determined by least squares fitting the detector image to the reference detector image. This registration process reduces clutter and jitter noise to a level comparable to the electronic noise level of the detector system. Test results with and without electronic noise using an analytical test function are presented.

Key Words: image, registration, least squares, clutter, jitter, array detector, satellite

THIS PAGE LEFT INTENTIONALLY BLANK.

TABLE OF CONTENTS

Section	Page
1 Introduction.....	9
2 Definition of the Problem	9
3 Analytical Representation of the Detector Image.....	11
4 Registration Algorithm for Known Transformation.....	13
5 Registration Algorithm for Unknown Transformation.....	15
6 Test Results.....	18
6.1 Test Images and Detector Signals.....	19
6.2 Detector Image Comparison	23
6.3 Test Registration with Known Transformation	26
6.4 Test Registration with Unknown Transformation	28
7 Appendix: Integrals and Partial Derivatives.....	32
8 Acknowledgments	37
9 References.....	39

THIS PAGE LEFT INTENTIONALLY BLANK.

LIST OF FIGURES

Figure		Page
Figure 1	A third or fourth order two-dimensional taylor series representation of the detector image function $G_k(x, y)$ centered on pixel m, n [Eq. (7)] is characterized by the pixel values $S_{k, m, n}^{measured}$ within the shaded region. A first or second order two-dimensional taylor series centered on pixel m, n is determined in terms of $S_{k, m, n}^{measured}$ values from pixels (m, n) , $(m, n + 1)$, $(m, n - 1)$, $(m + 1, n)$, $(m - 1, n)$	13
Figure 2	Three-dimensional mesh plot of the projected image function [Eq. (29)] resulting from the transformation T_1 . The p-pixels are along the x-direction and q-pixels are along the y-direction.	20
Figure 3	Three-dimensional mesh plot of the projected image function [Eq. (29)] resulting from the transformation T_2	20
Figure 4	Two-dimensional gray-scale plot of the projected image in Figure 2.	21
Figure 5	Two-dimensional gray-scale plot of the projected image in Figure 3.	21
Figure 6	Three-dimensional mesh plot of the pixel signal values $S_{1, m, n}^{test}$ [Eq. (31)] resulting from the transformation T_1	22
Figure 7	Three-dimensional mesh plot of the pixel signal values $S_{2, m, n}^{test}$ [Eq. (31)] resulting from the transformation T_2	22
Figure 8	Plot of $fd_{k, m, n}$ [Eq. (35)] versus pixel p, q for $S_{k, m, n}^{test}$ generated from Eq. (31) using T_1 assuming a second order taylor expansion for determining $S_{k, m, n}$	24
Figure 9	Plot of $fd_{k, m, n}$ [Eq. (35)] versus pixel p, q for $S_{k, m, n}^{test}$ generated from Eq. (31) using T_1 assuming a fourth order taylor expansion for determining $S_{k, m, n}$	24
Figure 10	Plot of $S_{1, m, n}$ with gaussian noise using a fourth order taylor expansion and transformation T_1	25
Figure 11	Plot of $fd_{k, m, n}$ corresponding to $S_{1, m, n}$ in Figure 10.	25
Figure 12	Plot of the fractional difference between the registered $S_{2, m, n}^{test}$ signal and the reference signal $S_{1, m, n}^{test}$ without noise. The maximum fractional difference shown here is 1.3×10^{-4} using a second order taylor expansion; the maximum fractional difference in this case (not shown) using a fourth order taylor expansion is 1.9×10^{-4}	27
Figure 13	Plot of the fractional difference between the registered $S_{2, m, n}^{test}$ signal and the reference signal $S_{1, m, n}^{test}$ both having uncorrelated noise (Sec. 6.2). The maximum fractional difference shown here is 0.27 using a fourth order taylor expansion. The maximum fractional difference in this case using a second order taylor expansion (not shown) is 0.26. The fractional difference can only be evaluated over those re-	

gions for which the registered $S_{2,m,n}^{test}$ and the reference signal $S_{1,m,n}^{test}$ overlap...27

- Figure 14 Plot of the displacement of the border pixels associated with each of the two subarrays centered on the detector array using the error matrix in Eq. (36). As the error matrix goes to zero, these points collapse to the origin.30
- Figure 15 Plot of the fractional difference between the registered $S_{2,m,n}^{test}$ signal and the reference signal $S_{1,m,n}^{test}$ without noise using a second order taylor expansion. The maximum fractional difference shown here is 1.2×10^{-4}30
- Figure 16 Plot of the fractional difference $fd_{k,m,n}$ between the registered $S_{2,m,n}^{test}$ signal using a second order taylor expansion and the reference signal $S_{1,m,n}^{test}$ with noise (0.02). The maximum value of $fd_{k,m,n}$ in this plot is 0.043.....31
- Figure 17 Plot of the fractional difference $fd_{k,m,n}$ between the registered $S_{2,m,n}^{test}$ using a fourth order taylor expansion and the reference signal $S_{1,m,n}^{test}$ with noise (0.02). The maximum value of $fd_{k,m,n}$ in this plot is 0.045.31

LIST OF TABLES

Table		Page
Table 1:	Zeroth, second, and fourth order λ -coefficients for Eqs. (10) - (11).....	12
Table 2:	Relative MATLAB Computational Costs.....	37

THIS PAGE LEFT INTENTIONALLY BLANK.

1 Introduction

This work was motivated by the need to be able to register satellite images of the earth as measured from different perspectives by an optical array detector for purposes of detecting and identifying random, localized optical events. An exact comparison between successive satellite images of the same earth scene is not possible because the satellite is never in the same position and orientation relative to the earth scene as time progresses. Fluctuations in individual detector pixel measurement values due to the regular, predictable motion of the satellite -- orbital, satellite sun and earth tracking -- are referred to as clutter noise. Jitter noise is attributed to random, unpredictable satellite motion such as angular motions due to tracking errors and equipment vibration. Clutter and jitter noise associated with individual pixel measurements over time periods on the order of seconds may be large compared to the detector shot and electronic noise.

The purpose of this paper is to present an algorithm that allows one to register images acquired from different perspectives. In this method the detector image is recovered from the discrete detector array signal values and represented over a local, continuous region by a fourth order, two-dimensional Taylor series (Sec. 3). This local detector image can then be registered by a general linear transformation with respect to a reference detector image. The detector signals in the reference frame can be reconstructed by integrating the registered detector image over each of the respective reference pixels. For the case in which the linear transformation is known, this image registration algorithm can be used to build a single extended image based upon a sequence of individual (partially overlapping) images acquired from various perspectives, or it can be used to look at differences between overlapping images taken at different times and perspectives (Sec. 4). Also, there are no practical constraints on the time dependence of the source image. In this case, the clutter noise is essentially eliminated. On the other hand, if the motion of the system is only partially known, due to the presence of jitter noise, so that the linear transformation is uncertain by no more than plus-or-minus two pixels over a subset of pixels, then the linear transformation is determined by least squares fitting the detector image to the reference image. Only a subset of pixel values are required for this least squares fit procedure; however, the number needed for convergence to a desired accuracy increases as the detector noise increases. The least squares fit procedure implicitly assumes that, in this case, the source image is essentially time independent except for occasional random optical events and electronic detector noise. This registration process can reduce clutter and jitter noise down to the electronic noise level of the detector system (Sec. 5). Test results for a 64×64 array detector with and without electronic noise using an analytical test function are presented in Sec. 6 [1].

A survey describing various other image registration techniques has been given by Brown [2]. Other algorithms for achieving subpixel registration have been given by Tian and Huhns [3] and Goshtasby, Stockman, and Page [4]. A contour-based approach to image registration has been developed by Li, Manjunath, and Mitra [5]. A least squares image registration algorithm has been indicated by Zikan [6]. In this paper the iterative solution to the integral equation (9) in Sec. 3 is central to our analytical registration method.

2 Definition of the Problem

Let the source image be $Q(u, v)$ and time independent for the purposes of this discussion (Sec. 2). Let $I_k(x, y)$ be the k th image that is projected on the array detector at relative time $k\Delta_t$. The x, y coordinates are attached to the array detector, and the origin of the x, y coordinate frame is

arbitrarily chosen to be the center of the array detector plane. The most general linear transformation [2, 7] between u, v and x, y is given by

$$u = A(t)x + B(t)y + C(t) \quad (1)$$

$$v = D(t)x + E(t)y + F(t) \quad (2)$$

and takes account of the changes in the detector image as a function of relative time t . Let $I_{k+1}(x, y)$ be the $(k+1)$ th image that is projected on the array detector at relative time $(k+1)\Delta_t$. During the time increment Δ_t the image projected onto the detector array may be rotated, scaled, sheared, displaced relative to the x, y coordinate frame due to sensor motion as implied in Eqs. (1) and (2). Equations (1) and (2) do not include the effects of perspective.

Now, consider the measured signals. Let $S_{k, m, n}$ be the analytical representation of the measured signal $S_{k, m, n}^{measured}$ at time $k\Delta_t$ from pixel m, n where

$$S_{k, m, n} = \int_{(n-1)\delta}^{no} \int_{(m-1)\delta}^{mo} I_k(x, y) dx dy \quad (3)$$

and δ is the width of a square detector pixel. The center coordinates of each pixel in terms of the indices m, n are given by

$$x_m = (m - 1/2)\delta \quad (4)$$

$$y_n = (n - 1/2)\delta \quad (5)$$

where m, n run from $(-N_{pixels}/2) + 1$ to $N_{pixels}/2$. N_{pixels} is the total number of pixel rows or columns and is assumed to be even. The analytical signal from pixel m, n at time $k'\Delta_t$ is $S_{k', m, n}$ where

$$S_{k', m, n} = \int_{(n-1)\delta}^{no} \int_{(m-1)\delta}^{mo} I_{k'}(x, y) dx dy \quad (6)$$

Clearly, if the image has been rotated, scaled, sheared, displaced relative to the x, y coordinate frame in the time interval Δ_t , then $I_k(x, y)$ and $I_{k'}(x, y)$ are functionally different and the signal $S_{k', m, n}$ is different from the signal $S_{k, m, n}$ even though the source image has not changed. Therefore, the problem here is that signal $S_{k', m, n}$ does not *register* with signal $S_{k, m, n}$.

The purpose of this paper is to define an algorithm that transforms the signal $S_{k', m, n}$ so that it can be *registered* with another signal such as $S_{k, m, n}$.

3 Analytical Representation of the Detector Image

The effects of detecting the optical image by an array detector consisting of $N_{pixels} \times N_{pixels}$ square detector pixels of width δ [8] is equivalent to applying a spatial frequency filter to the projected image function $I_k(x, y)$. Thus, the *detector* image $G_k(x, y)$ corresponds to the spatial frequency filtered projected image function. If the point spread function of the optical system is comparable or greater than the dimensions of a detector pixel, then the projected image function $I_k(x, y)$ and the detector image function $G_k(x, y)$ are essentially the same and the overall resolution of the system is consistent. These effects are exemplified in Sec. 6.

The detector image $G_k(x, y)$ at time $k\Delta_t$, that can be deduced from $S_{k, m, n}^{measure}$, is represented over a local region by a two-dimensional Taylor expansion

$$G_k(x, y) = G_{k, m, n} + \left. \frac{\partial G}{\partial x} \right|_{k, m, n} (x - x_m) + \left. \frac{\partial G}{\partial y} \right|_{k, m, n} (y - y_n) + \dots \quad (7)$$

where

$$G_{k, m, n} \equiv G_k(x_m, y_n) . \quad (8)$$

In our analysis $G_k(x, y)$ is carried out to fourth order [only the zero and first order terms are shown in Eq. (7)]. The detector image $G_k(x, y)$ is related to the pixel signal $S_{k, m, n}$ by

$$S_{k, m, n} = \int_{(n-1)\delta}^{no} \int_{(m-1)\delta}^{mo} G_k(x, y) dx dy . \quad (9)$$

Substitution of Eq. (7) for $G_k(x, y)$ into Eq. (9) yields

$$S_{k, m, n} = \delta^2 [\lambda_0 G_{k, m, n} + \Psi_{k, m, n}] \quad (10)$$

where

$$\begin{aligned} \Psi_{k, m, n} = & \lambda_1 [G_{k, m+2, n} + G_{k, m-2, n} + G_{k, m, n+2} + G_{k, m, n-2}] \\ & + \lambda_2 [G_{k, m+1, n} + G_{k, m-1, n} + G_{k, m, n+1} + G_{k, m, n-1}] \\ & + \lambda_3 [G_{k, m+1, n+1} + G_{k, m+1, n-1} + G_{k, m-1, n+1} + G_{k, m-1, n-1}] . \end{aligned} \quad (11)$$

Values for λ_j are tabulated in Table 1. Odd order contributions from Eq. (7) in Eq. (9) are zero.

In this analysis the partial derivatives $\left. \frac{\partial^r G}{\partial x^{r-s} \partial y^s} \right|_{k, m, n}$ in Eq. (7) are expressed in terms of finite differences so that, for example,

Table 1: Zeroth, second, and fourth order λ -coefficients for Eqs. (10) - (11).

Order	λ_0	λ_1	λ_2	λ_3
0th	1	0	0	0
2nd	5/6	0	1/24	0
4th	1219/1440	1/1920	13/360	1/576

$$\left. \frac{\partial G}{\partial y} \right|_{k,m,n} = \frac{G_{k,m,n+1} - G_{k,m,n-1}}{2\delta}. \quad (12)$$

Consequently, all partial derivatives in Eq. (7) are replaced by various linear combinations of $G_{k,i,j}$ as defined in Eq. (8).

The $G_{k,m,n}$ can be evaluated according to the following algorithm.

Step 1: The $G_{k,m,n}$ are given to zeroth order by

$$G_{k,m,n} = \frac{S_{k,m,n}^{measured}}{\delta^2}. \quad (13)$$

Step 2: To a higher order approximation consistent with Eqs. (7) and (9), the $G_{k,m,n}$ are given by

$$G_{k,m,n} = \frac{1}{\lambda_0} \left[\frac{S_{k,m,n}^{measured}}{\delta^2} - \Psi_{k,m,n} \right]. \quad (14)$$

Using the previous values of $G_{k,m,n}$ to evaluate the perturbing term $\Psi_{k,m,n}$, new values of $G_{k,m,n}$ are given by Eq. (14). A self-consistent solution is found by iterating Eq. (14) for all allowed values of m,n . The rate of convergence is such that the maximum absolute fractional change in $G_{k,m,n}$ decreases by about an order of magnitude for each iteration. The zeroth order solution gives values of $G_{k,m,n}$ for $1 \leq m \leq N_{pixels}$ and $1 \leq n \leq N_{pixels}$, the second order solution gives values of $G_{k,m,n}$ for $1 < m < N_{pixels}$ and $1 < n < N_{pixels}$, and the fourth order solution gives values of $G_{k,m,n}$ for $2 < m < N_{pixels} - 1$ and $2 < n < N_{pixels} - 1$. It is computationally cost effective to first determine the second order solution and then proceed with the fourth order solution as opposed to doing only a fourth order solution starting with the zeroth order values for $G_{k,m,n}$.

At this point, we now have a functional representation of the detector image $G_k(x, y)$ as represented by Eq. (7) in the vicinity of x_m, y_n as deduced from measured values of $S_{k,m,n}^{measured}$. The neighborhood over which the two-dimensional taylor series representation of the image extends is shown by the shaded region in Figure 1.

With respect to the performance of an actual optical system, it is important that the optical system itself be free of asymmetric astigmatism if image registration is anticipated. Circularly symmetric optical blur spots should not be a problem. Also, it may be necessary to correct the signal pixel values in order to account for any significant differences in their respective sensitivity. The analysis presented in this paper assumes linear optics [Eqs. (1) and (2)]; however, these trans-

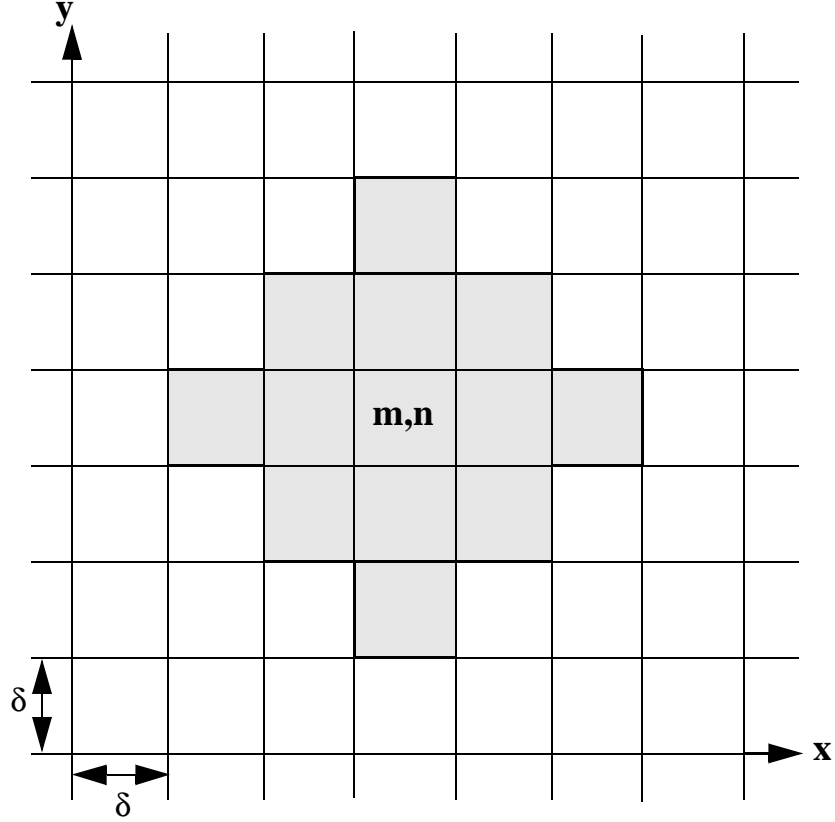


Figure 1 A third or fourth order two-dimensional Taylor series representation of the detector image function $G_k(x, y)$ centered on pixel m, n [Eq. (7)] is characterized by the pixel values $S_{k, m, n}^{measured}$ within the shaded region. A first or second order two-dimensional Taylor series centered on pixel m, n is determined in terms of $S_{k, m, n}^{measured}$ values from pixels $(m, n), (m, n + 1), (m, n - 1), (m + 1, n), (m - 1, n)$.

formation equations could be extended, at least in principle, to account for some nonlinear optical effects.

4 Registration Algorithm for Known Transformation

This image registration algorithm (Sec. 4) can be used to build a single extended image based upon a sequence of individual partially overlapping images acquired from various perspectives, or it can be used to look at differences between overlapping images taken at different times and perspectives. Also, it can be used to generate images from a given reference image for specified T_k for simulation purposes. This algorithm (Sec. 4) assumes that the transformation matrix T_k can be specified either theoretically or from measurements of the system's motion.

The coordinate transformation between source point u, v and image point x, y in the focal plane of the detector at relative time $k\Delta_t$ is T_k where

$$\begin{bmatrix} u \\ v \\ 1 \end{bmatrix} = T_k \begin{bmatrix} x \\ y \\ 1 \end{bmatrix} = \begin{bmatrix} A(k\Delta_t) & B(k\Delta_t) & C(k\Delta_t) \\ D(k\Delta_t) & E(k\Delta_t) & F(k\Delta_t) \\ 0 & 0 & 1 \end{bmatrix} \begin{bmatrix} x \\ y \\ 1 \end{bmatrix}. \quad (15)$$

Since the x,y coordinate frame is attached to the array detector, the transformation T_k causes rotation, scaling, shearing, and displacement of the image with respect to the x,y coordinates as a function of time. Here, T_k is assumed to be known for all k .

In this discussion, the source image $Q_k(u, v)$ may be time dependent. Let $G_R(X, Y)$ be a reference image that is related to the source image at relative time $R\Delta_t$ by the transformation T_R . X, Y are the reference frame coordinates and simply correspond to the x, y coordinates at relative time $R\Delta_t$. Suppose that one wants to *register* other images with respect to this reference image. If T_k transforms the source image $Q_k(u, v)$ to the detector image $G_k(x, y)$, then $T_k^{-1}T_R$ transforms the detector image $G_k(x, y)$ to an image $H_k(X, Y)$ in the reference coordinate frame where

$$\begin{bmatrix} x \\ y \\ 1 \end{bmatrix} = T_k^{-1}T_R \begin{bmatrix} X \\ Y \\ 1 \end{bmatrix} = T_{k,R} \begin{bmatrix} X \\ Y \\ 1 \end{bmatrix}. \quad (16)$$

(This can be verified using a simple analytical function for $Q_k(u, v)$ and arbitrary linear transformations for T_R and T_k .) $G_k(x, y)$ is represented in terms of a two dimensional Taylor series [Eq. (7)] which represents the detector image over a limited spatial region (Figure 1) about the point x_m, y_n . The same image in the reference coordinate frame $H_k(X, Y)$ is valid in a transformed region [9] about the point ξ_k, ζ_k in the X, Y reference plane where

$$\begin{bmatrix} \xi_k \\ \zeta_k \\ 1 \end{bmatrix} = T_R^{-1}T_k \begin{bmatrix} x_m \\ y_n \\ 1 \end{bmatrix} = T_{R,k} \begin{bmatrix} x_m \\ y_n \\ 1 \end{bmatrix}. \quad (17)$$

An analytical representation of $H_k(X, Y)$ in terms of $G_k(x, y)$ is given in the Appendix. The M_k, N_k indices in the X, Y reference plane which contain the center of convergence ξ_k, ζ_k are given by

$$M_k = \text{ceil}(\xi_k/\delta) \quad (18)$$

$$N_k = \text{ceil}(\zeta_k/\delta) \quad (19)$$

where the operator *ceil* rounds a floating point number towards plus infinity to an integer. These indices are consistent with the definitions in Eqs. (4) and (5). The transformation $T_{R,k}$ can be used to transform the region in Figure 1 to the corresponding region in the reference coordinate frame.

The registered signal value $S_{k,M,N}^{reg}$ associated with pixel M_k, N_k in the reference coordinate frame corresponding to $G_k(x, y)$ is given by

$$S_{k, M, N}^{reg} = \int_{(N-1)\delta}^{N\delta} \int_{(M-1)\delta}^{M\delta} H_k(X, Y) dXdY . \quad (20)$$

Depending upon how T_k changes with time, $S_{k, M, N}^{reg}$ may not completely overlap with $S_{R, M, N}^{ref}$ and may extend beyond the boundaries of $S_{R, M, N}^{ref}$. The order of the Taylor expansion must be sufficient for $H_k(X, Y)$ to accurately span the area of integration in Eq. (20). This also implies that there are practical limitations on $T_{R, k}$. Registration of an image can result in the loss of information. This can occur, for example, if the image projected on the array detector undergoes contraction (for example, due to increasing distance between source and detector).

5 Registration Algorithm for Unknown Transformation

Motion of the optical sensor with respect to the source image that is predictable gives rise to clutter noise as measured by the array detector due to the motion of the projected image having lateral contrast relative to the array detector. For example, an array detector zooming in on a static source image would give various measurement values because the image projected on the array detector would be expanding. Similarly, motion of the optical sensor with respect to the source image that is random and unpredictable, such as system angular vibrational motion, gives rise to jitter noise.

We now consider the problem in which T_k is not completely known. In particular, two kinds of motion may coexist: motion that is predictable and motion that is random. In this registration algorithm, the predictive motion between time steps may be large, but the random motion must be small. This method is based on a least squares fit procedure that is used to determine the optimum transformation for purposes of registering a detector image with respect to a reference image. This algorithm can be applied to situations in which an optical array detector makes successive measurements from different vantage points of a source scene that is essentially time independent except for occasional random optical events in time and location. The measured signals $S_{k, m, n}^{measured}$ may also include detector noise. As a result of the registration process, contributions to clutter and jitter noise within $S_{k, m, n}^{measured}$ are typically reduced to the detector noise level. The least squares algorithm is as follows.

Step 1: Pixel Selection. For the k th detector image, select pixels m, n whose signal values $S_{k, m, n}^{measured}$ are to be used in the least squares fit procedure. As the least squares fit progresses, alternative pixels may be used for successive iterations. At each iteration, the pixels in the reference frame may need to be matched, if necessary, to the pixels selected in the k th detector image due to changes in the transformation matrix with each least squares fit iteration. Only those pixels that overlap with the reference array are included in the least squares fit procedure. Within a square subarray which typically excludes several of the outer rows, we pick every N_{skip} pixel. If convergence fails, another subset of pixels is chosen by picking every $N_{skip}/2$ pixel. A starting value of $N_{skip} = 16$ is reasonable. It may be necessary for the user to experiment with the number of pixels needed in order to get a sufficiently accurate least squares fit; the number of pixels

needed in the least squares fit will depend upon the degree of lateral contrast in the detector image and the level of detector noise relative to the lateral variation in $S_{k,m,n}^{measured}$.

Step 2: $G_{k,m,n}$. From the measured values $S_{k,m,n}^{measured}$, the detector image values $G_{k,m,n}$ are determined as indicated in Sec. 3. The values of $G_{k,m,n}$ and x_m, y_n define the two-dimensional Taylor series [Eq. (7)] that is an analytical representation of the detector image $G_k(x, y)$ in the neighborhood of x_m, y_n (see Figure 1) at relative time $k\Delta_t$.

Step 3: $T_{k,R}$. The user must supply an initial guess for the effective transformation $T_{k,R}$ defined in Eq. (16). Even though $T_{k,R}$ may result in significant displacement of the pixels with respect to their original positions, $T_{k,R}$ must position the image with respect to the reference image to within plus-or-minus two pixels. If Δ_t is sufficiently small, then $T_{k-1,R}$, which is known from the previous least squares fit, can be used as the initial guess for $T_{k,R}$. Another approach might be to calculate $T_{k,R}$ based on the known kinematics of the system. All of the known movements of the system, which give rise to clutter noise and may give rise to large displacements, are represented by $K_{k,R}$; presumed values for the matrix elements of $K_{k,R}$ can be calculated or deduced from measurement. The unknown movements of the system which give rise to jitter noise must be small and are represented by $J_{k,R}$. Since $J_{k,R}$ is unknown, it might be approximated by either zero motion matrix elements or the previous value $J_{k-1,R}$, providing the present value has some correlation with the previous value. Thus, the estimated value for $T_{k,R}^{est}$ is given symbolically by

$$T_{k,R}^{est} = K_{k,R}^{cal} J_{k,R}^{est}. \quad (21)$$

The estimated transformation matrix $T_{k,R}^{est}$ must bring the pixels chosen within the subarray to within plus-or-minus two pixels of being correctly registered assuming a third or fourth order Taylor series representation of $G_k(x, y)$ or within plus-or-minus one pixel of being correctly registered assuming either a first or second order Taylor expansion. Otherwise, convergence of the least squares fit procedure may be impossible.

Step 4: $S_{k,M,N}$. Having $T_{k,R}$ or $T_{k,R}^{est}$ allows one to transform the detector image $G_k(x, y)$ to its corresponding image $H_k(X, Y)$ in the reference frame. The general analytical expression for $H_k(X, Y)$ is given in the Appendix. The two-dimensional Taylor series in the reference coordinate frame is expanded about ξ_k, ζ_k as given by Eq. (17); this point is contained within the reference pixel M_k, N_k specified by Eqs. (18) - (19). The calculated values for $S_{k,M,N}^{reg}$ with respect to the reference array are given by Eq. (20). The analytical expression for $S_{k,M,N}^{reg}$ as well as the partial derivatives of $S_{k,M,N}^{reg}$ with respect to the $T_{k,R}$ transformation parameters $A_{k,R}, B_{k,R}, C_{k,R}, D_{k,R}, E_{k,R}, F_{k,R}$ are given in the Appendix.

Step 5: Least Squares Fit Equations. Given that

$$U_{p,q} = \sum_{n=1}^{i^{data}} \frac{\partial S_{k,M_n,N_n}^{reg}}{\partial \chi_p} \frac{\partial S_{k,M_n,N_n}^{reg}}{\partial \chi_q} \quad (22)$$

$$V_p = \sum_{n=1}^{i^{data}} (S_{R,M_n,N_n}^{ref} - S_{k,M_n,N_n}^{reg}) \frac{\partial S_{k,M_n,N_n}^{ref}}{\partial \chi_p} \quad (23)$$

where $S_{k,M,N}^{reg}$ is determined from Eq. (20), the sum over n is over the M_n, N_n pixels selected which can be registered with respect to the reference image. The parameter χ_j corresponds to the j th element in the sequence of transformation elements $A_{k,R}, B_{k,R}, C_{k,R}, D_{k,R}, E_{k,R}, F_{k,R}$ in Eq.

(15). The analytical expressions for $S_{k,M,N}^{reg}$ and $\frac{\partial S_{k,M_n,N_n}^{reg}}{\partial \chi_p}$ are given in the Appendix. The idea is to least squares fit $S_{k,M,N}^{reg}$ to S_{R,M_n,N_n}^{ref} as a function of $A_{k,R}, B_{k,R}, C_{k,R}, D_{k,R}, E_{k,R}, F_{k,R}$. This implies that $S_{k,M,N}^{reg}$ must have some semblance to S_{R,M_n,N_n}^{ref} . Hence, this algorithm applies to source scenes which are for the most part time independent. This does not exclude having detector noise, and $S_{k,M,N}^{reg}$ may be perturbed by occasional random optical events; however, it is better to exclude pixels from the least squares process having obvious transient optical signal values.

The corrections to the transformation parameters $A_{k,R}, B_{k,R}, C_{k,R}, D_{k,R}, E_{k,R}, F_{k,R}$ are found by solving the linear matrix equation

$$U\mathbf{c} = \mathbf{V} \quad (24)$$

for \mathbf{c} so that $A_{k,R} = A_{k,R} + c_1, \dots, F_{k,R} = F_{k,R} + c_6$. Steps 4 and 5 are repeated until

$$\max\left(\frac{\text{absolute}(c_p)}{\text{absolute}(\chi_p) + \text{eps}}\right) < \text{Epsilon} . \quad (25)$$

where *Epsilon* has a value on the order of 10^{-4} and *eps* is set to a small number (10^{-6}).

Step 6: Image Registration. After the transformation $T_{k,R}$ has been determined, the total image can be registered with respect to the reference array by Eq. (20) giving $S_{k,M,N}^{reg}$ with clutter and jitter noise contributions ideally reduced to the detector noise level. Optical events of interest may now more readily be detected by taking the difference between $S_{k,M,N}^{reg}$ and $S_{R,M,N}^{ref}$.

6 Test Results

In order to exemplify these algorithms, the optical source function $Q^{test}(u, v)$ was arbitrarily represented by the test function

$$Q^{test}(u, v) = 3 + \cos(\mu u) + \cos(\varphi v) \quad (26)$$

where

$$\mu = \frac{2\pi}{91.4\delta} \quad (27)$$

$$\varphi = \frac{2\pi}{40.74\delta} \quad (28)$$

and δ is the width of the detector square pixels. The projected image function $I_k^{test}(x, y)$ is given by

$$I_k^{test}(x, y) = 3 + \cos[\mu(A_k x + B_k y + C_k)] + \cos[\varphi(D_k x + E_k y + F_k)] \quad (29)$$

The numerical values for μ and φ have been chosen so that the variation in $I_k^{test}(x, y)$ over a pixel width is small (the detector image is consistent with the projected image). This condition is fulfilled for

$$\begin{bmatrix} \mu \\ \varphi \end{bmatrix} T_{k,i,j} \delta / 2 \ll \begin{bmatrix} 1 \\ 1 \end{bmatrix} \quad (30)$$

where i, j range from 1 to 2 as deduced from Eq. (31). This function can be integrated exactly for any value of μ and φ to give the test pixel signal values $S_{k,m,n}^{test}$ where

$$\begin{aligned} S_{k,m,n}^{test} &= 3\delta^2 \\ &+ \delta^2 \frac{\sin \frac{\mu A_k \delta}{2} \sin \frac{\mu B_k \delta}{2}}{\frac{\mu A_k \delta}{2} \frac{\mu B_k \delta}{2}} \cos \{ \mu [A_k \delta (m - 1/2) + B_k \delta (n - 1/2) + C_k] \} \\ &+ \delta^2 \frac{\sin \frac{\varphi D_k \delta}{2} \sin \frac{\varphi E_k \delta}{2}}{\frac{\varphi D_k \delta}{2} \frac{\varphi E_k \delta}{2}} \cos \{ \varphi [D_k \delta (m - 1/2) + E_k \delta (n - 1/2) + F_k] \} \quad (31) \end{aligned}$$

The *sinc* functions in front of the *cos* functions in Eq. (31) correspond to the effects of spatial frequency filtering inherent in the array detector. The numerical values arbitrarily chosen for the transformation matrices were

$$T_1 = \begin{bmatrix} 0.9 & 0.31 & 3.1\delta \\ -0.351 & 0.95 & -3.3\delta \\ 0 & 0 & 1 \end{bmatrix}, \quad (32)$$

$$T_2 = \begin{bmatrix} 0.757 & -0.737 & 6\delta \\ 0.807 & 0.607 & -7\delta \\ 0 & 0 & 1 \end{bmatrix}, \quad (33)$$

from which

$$T_{2,1} = \begin{bmatrix} 0.755309 & 0.876204 & -8.89786\delta \\ -0.702019 & 0.468946 & 9.92659\delta \\ 0 & 0 & 1 \end{bmatrix}. \quad (34)$$

The fictitious array detector was characterized by $N_{pixels} = 64$ and $\delta = 100$ microns.

6.1 Test Images and Detector Signals

Three-dimensional mesh plots of the projected images [Eq. (29)] derived from T_1 and T_2 are shown in Figure 2 and Figure 3, respectively. The two-dimensional gray-scale plot of each image (Figure 2 and Figure 3) is shown in Figure 4 and Figure 5, respectively. Plots of the pixel signal values $S_{k,m,n}^{test}$ [Eq. (31)] for T_1 and T_2 are shown in Figure 6 and Figure 7, respectively, and are essentially the same as those of the respective projected images aside from a scaling factor of δ^2 .

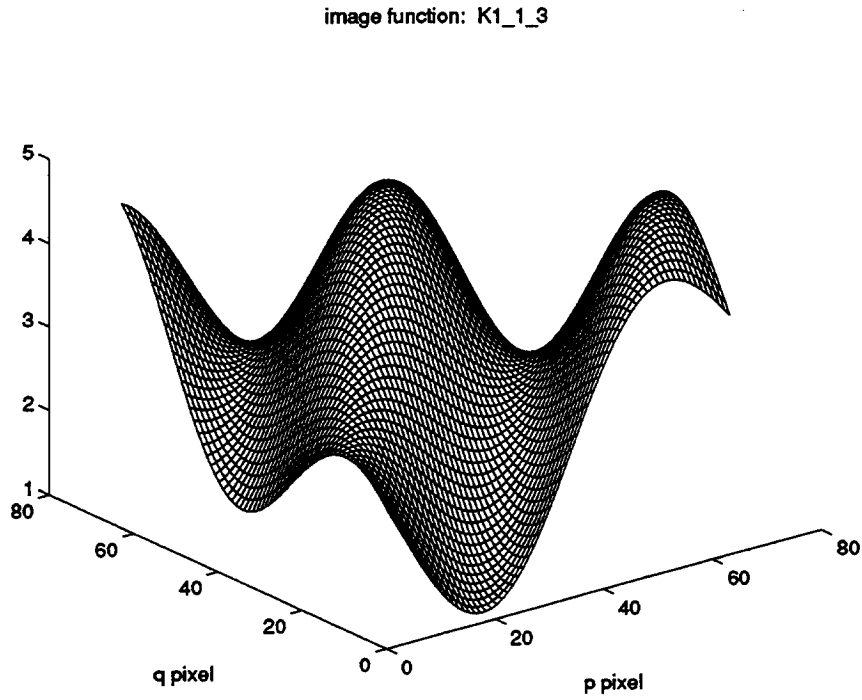


Figure 2 Three-dimensional mesh plot of the projected image function [Eq. (29)] resulting from the transformation T_1 . The p-pixels are along the x-direction and q-pixels are along the y-direction.

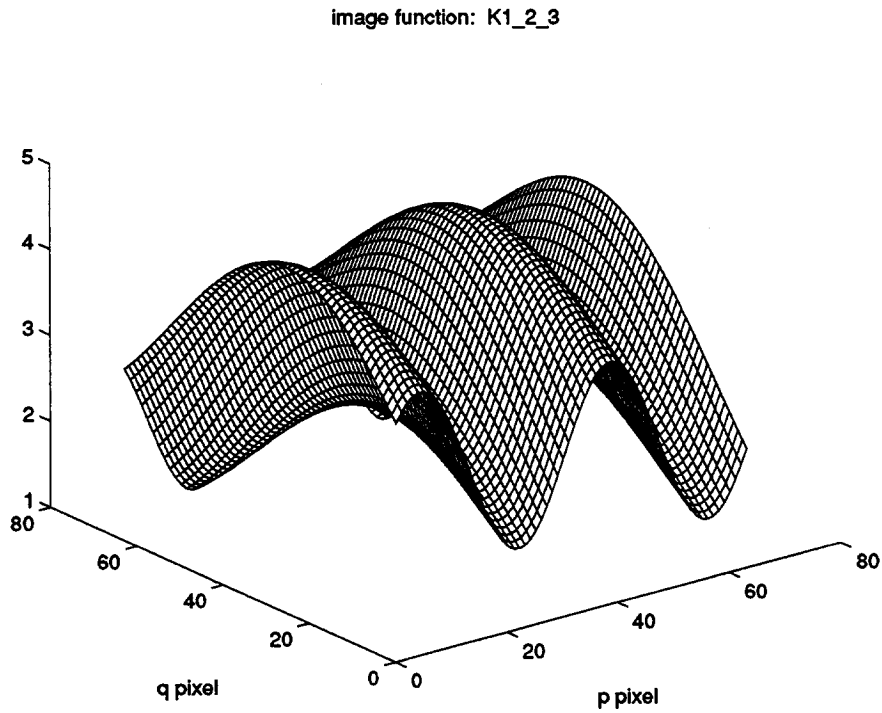


Figure 3 Three-dimensional mesh plot of the projected image function [Eq. (29)] resulting from the transformation T_2 .

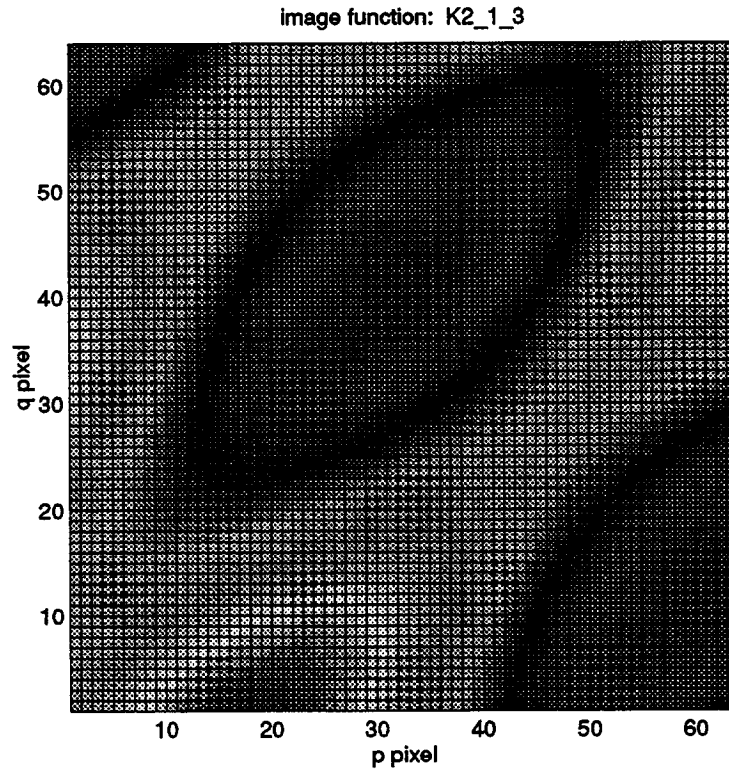


Figure 4 Two-dimensional gray-scale plot of the projected image in Figure 2.

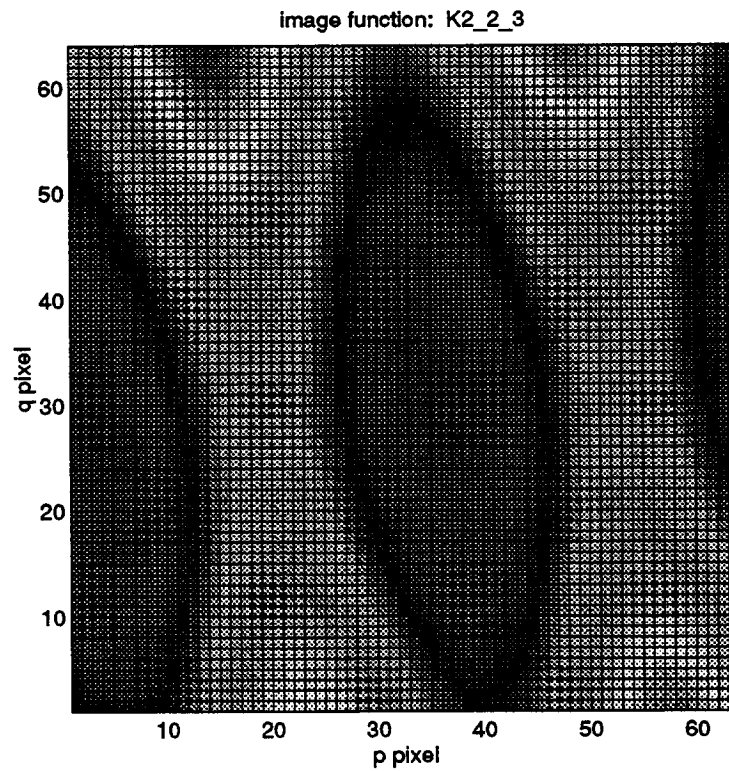


Figure 5 Two-dimensional gray-scale plot of the projected image in Figure 3.

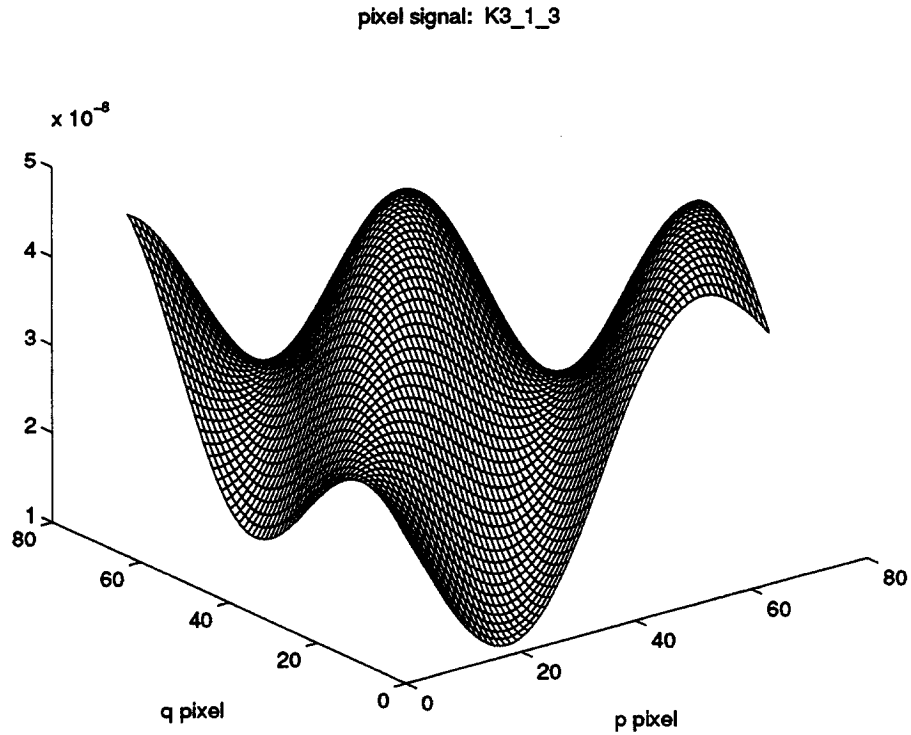


Figure 6 Three-dimensional mesh plot of the pixel signal values $S_{1,m,n}^{test}$ [Eq. (31)] resulting from the transformation T_1 .

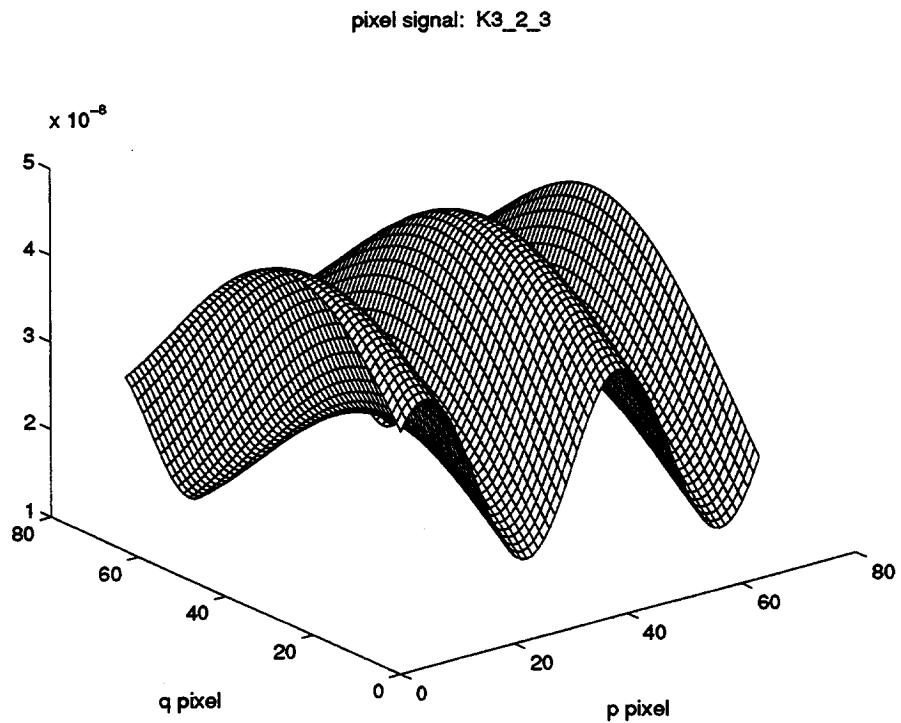


Figure 7 Three-dimensional mesh plot of the pixel signal values $S_{2,m,n}^{test}$ [Eq. (31)] resulting from the transformation T_2 .

6.2 Detector Image Comparison

The fractional difference $fd_{k,m,n}$ between signal value $S_{k,m,n}$ as deduced numerically from the algorithm in Sec. 3 and the test signal value $S_{k,m,n}^{test}$ [Eq. (31)], which was determined exactly from the test image source function $Q^{test}(u, v)$, is given by

$$fd_{k,m,n} = \frac{S_{k,m,n} - S_{k,m,n}^{test}}{S_{k,m,n}^{test}}. \quad (35)$$

The results of this computation are shown in Figure 8 and Figure 9 for second and fourth order Taylor expansions and indicate the error in determining $S_{k,m,n}$ according to the algorithm in Sec. 3. The higher order representation extends the area over which $G_k(x, y)$ is represented. The accuracy is limited by the approximations implicit in Eqs. (10) and (11) (namely representing the partial derivatives in the Taylor series by finite differences). The values for $fd_{k,m,n}$ increase as the spatial rate of change in $Q^{test}(u, v)$ increases (by increasing the values for μ and ϕ).

The effects of noise have also been explored. Gaussian noise was added to $S_{k,m,n}^{test}$, which is shown in Figure 10. The standard deviation in this noise was defined to be 0.1 times the minimum value of $S_{k,m,n}^{test}$, which ranges between approximately δ^2 and $5\delta^2$ according to Eq. (31). The fractional difference $fd_{k,m,n}$ between $S_{k,m,n}$, as deduced from $S_{k,m,n}^{test}$ with noise according to the algorithm in Sec. 3, and the noisy $S_{k,m,n}^{test}$ is shown in Figure 11.

fractional difference: O2_2_3

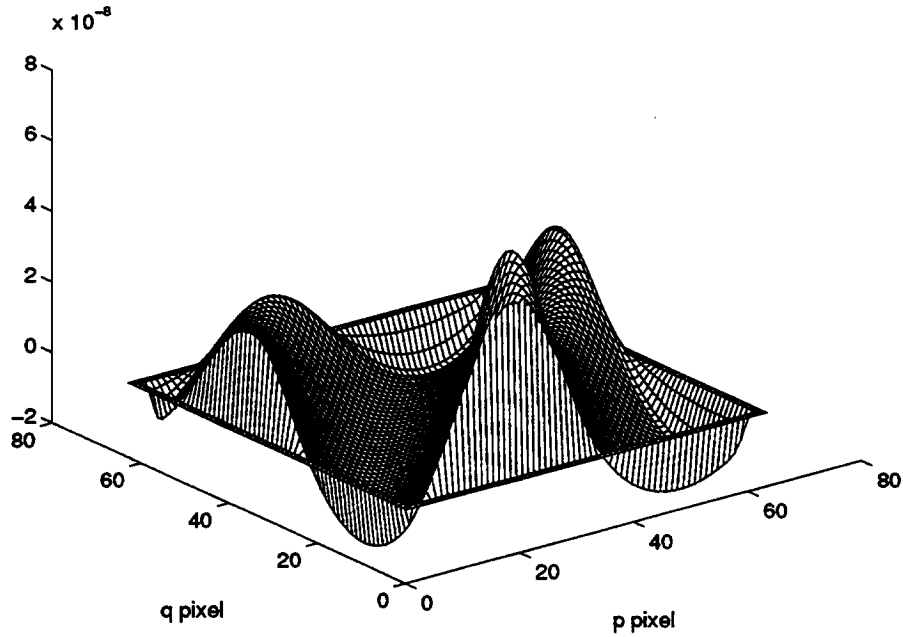


Figure 8 Plot of $fd_{k,m,n}$ [Eq. (35)] versus pixel p,q for $S_{k,m,n}^{test}$ generated from Eq. (31) using T_1 assuming a second order taylor expansion for determining $S_{k,m,n}$.

fractional difference: O2_4_3

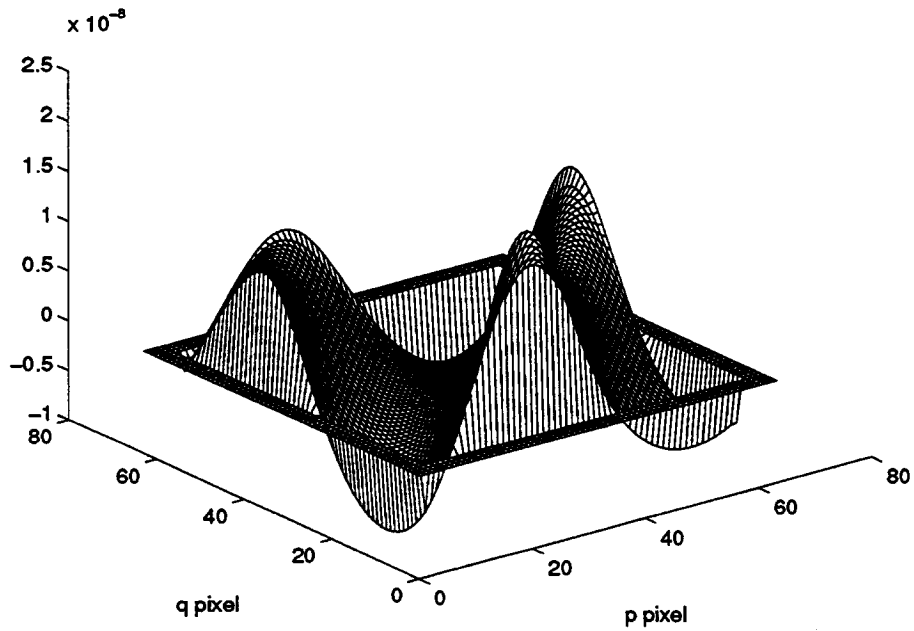


Figure 9 Plot of $fd_{k,m,n}$ [Eq. (35)] versus pixel p,q for $S_{k,m,n}^{test}$ generated from Eq. (31) using T_1 assuming a fourth order taylor expansion for determining $S_{k,m,n}$.

numerical S: O1_4_37

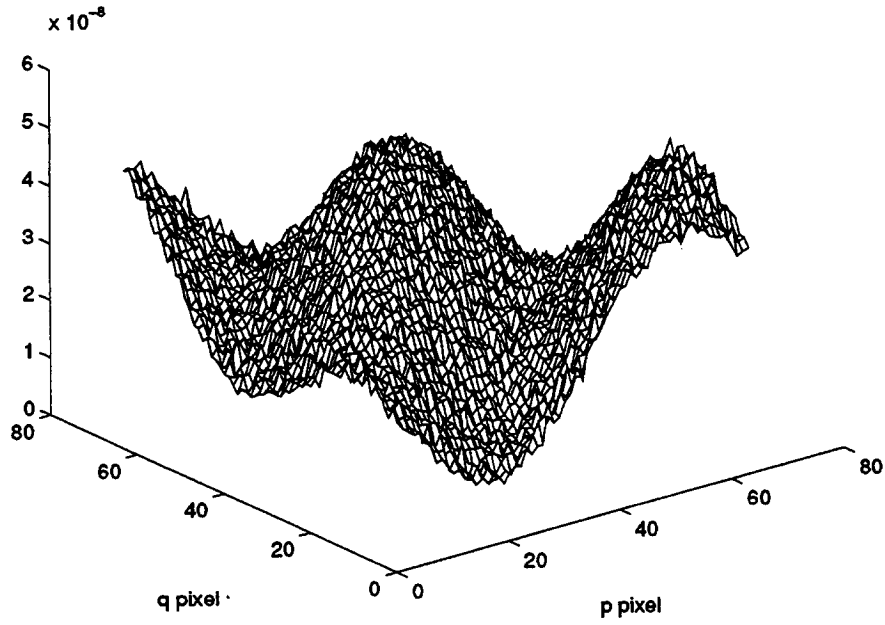


Figure 10 Plot of $S_{1,m,n}$ with gaussian noise using a fourth order taylor expansion and transformation T_1 .

fractional difference: O2_4_37

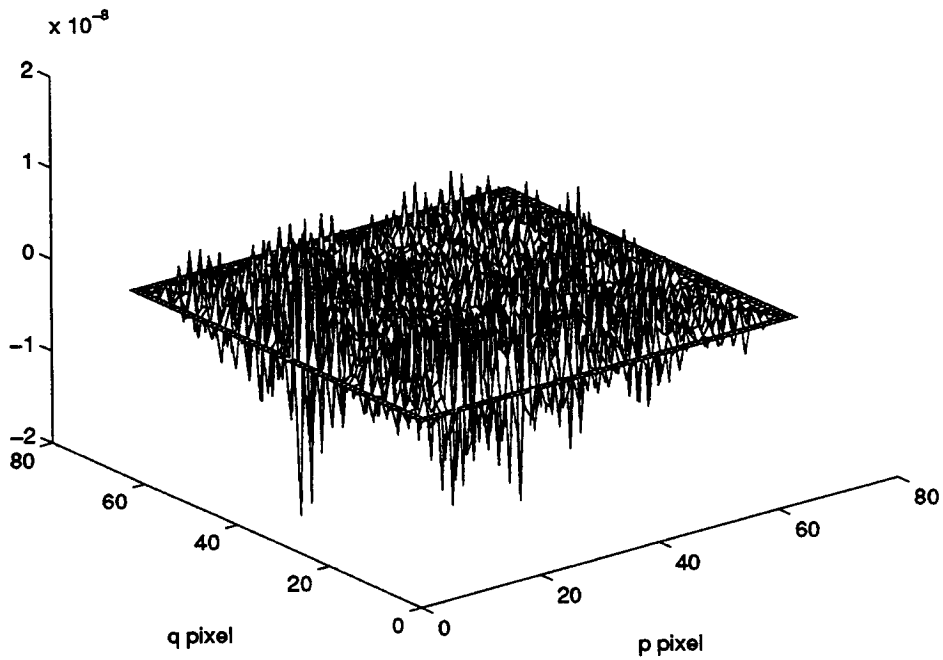


Figure 11 Plot of $fd_{k,m,n}$ corresponding to $S_{1,m,n}$ in Figure 10.

6.3 Test Registration with Known Transformation

The signal $S_{2,m,n}^{test}$ shown in Figure 7 was registered to the reference signal $S_{1,m,n}^{test}$ shown in Figure 6 using the algorithm in Sec. 4. In this case the transformation is known [Eq. (34)]. The quality of the registration is measured in terms of the fractional difference $fd_{k,m,n}$ between the registered signal and the reference signal. This fractional differences $fd_{k,m,n}$ is shown in Figure 12. Without noise, the fractional difference in the signals is on the order of 10^{-5} to 10^{-4} .

An analogous plot was made for the registration of $S_{2,m,n}^{test}$ with noise to the reference signal $S_{1,m,n}^{test}$ shown in Figure 10. Both signals have the same level of (uncorrelated) noise (0.1, Sec. 6.2). Now the fractional difference in the registered and reference signal closely approaches as expected the gaussian noise level as shown in Figure 13.

fractional difference: L2_2_3

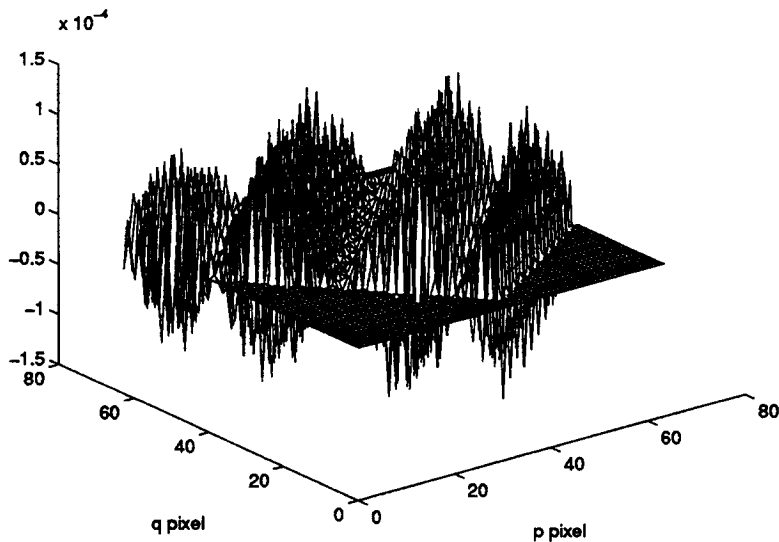


Figure 12 Plot of the fractional difference between the registered $S_{2,m,n}^{test}$ signal and the reference signal $S_{1,m,n}^{test}$ without noise. The maximum fractional difference shown here is 1.3×10^{-4} using a second order taylor expansion; the maximum fractional difference in this case (not shown) using a fourth order taylor expansion is 1.9×10^{-4} .

fractional difference: L2_4_37

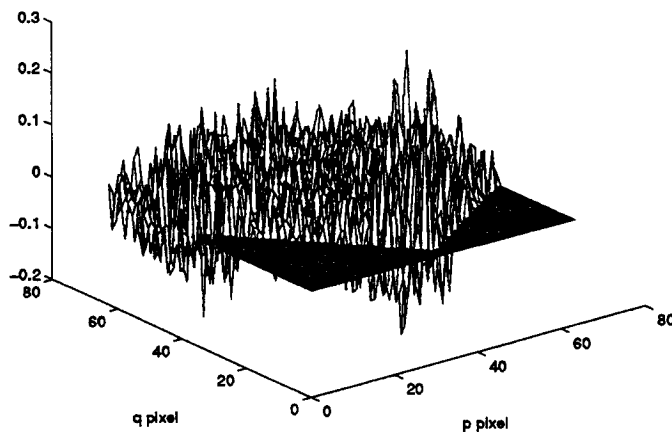


Figure 13 Plot of the fractional difference between the registered $S_{2,m,n}^{test}$ signal and the reference signal $S_{1,m,n}^{test}$ both having uncorrelated noise (Sec. 6.2). The maximum fractional difference shown here is 0.27 using a fourth order taylor expansion. The maximum fractional difference in this case using a second order taylor expansion (not shown) is 0.26. The fractional difference can only be evaluated over those regions for which the registered $S_{2,m,n}^{test}$ and the reference signal $S_{1,m,n}^{test}$ overlap.

6.4 Test Registration with Unknown Transformation

The signal $S_{2,m,n}^{test}$ shown in Figure 7 was registered to the reference signal $S_{1,m,n}^{test}$ shown in Figure 6 using the algorithm in Sec. 5. In this case the required transformation is supposedly unknown. In order for the least squares fit algorithm in Sec. 5 to converge, the transformation must be partially known at least to the extent that it will bring those pixel signal values chosen for the least squares fit procedure to within plus-or-minus two pixels of being registered. The known transformation in Eq. (34) was perturbed by adding to it the error matrix

$$T_{error} = \begin{bmatrix} 0.05 & -0.08 & -1.5\delta \\ 0.04 & 0.04 & 1.5\delta \\ 0 & 0 & 0 \end{bmatrix}. \quad (36)$$

The displacement of the border pixels associated with the square array $N_{pixel}/4 \times N_{pixel}/4$ and $N_{pixel}/2 \times N_{pixel}/2$ centered on the array detector due to just T_{error} is shown in Figure 14.

For the case in which $S_{1,m,n}^{test}$ and $S_{2,m,n}^{test}$ are free of noise, the least squares fit procedure using the second order taylor expansion converged in five iterations yielding

$$T_{LSF} = \begin{bmatrix} 0.755309 & 0.876211 & -8.89785\delta \\ -0.702021 & 0.468944 & 9.92663\delta \\ 0 & 0 & 1 \end{bmatrix}. \quad (37)$$

The correct answer is given by Eq. (34) so that the residual error is

$$T_{error} = T_{LSF} - T_{2,1} = \begin{bmatrix} 0.0 & 0.000007 & 0.00001\delta \\ -0.000002 & -0.000002 & 0.00004\delta \\ 0 & 0 & 0 \end{bmatrix}. \quad (38)$$

The results of this least squares fit in terms of the fractional difference between the registered $S_{2,m,n}^{test}$ signal and the reference $S_{1,m,n}^{test}$ signal is shown in Figure 15.

Next, we consider the registration of $S_{2,m,n}^{test}$ onto the reference signal $S_{1,m,n}^{test}$ for the case in which both signals are noisy (Sec. 6.3). The standard deviation in this noise was defined to be 0.02 times the minimum value of $S_{k,m,n}^{test}$. The least squares fit using the second order taylor expansion converged in sixteen iterations yielding

$$T_{LSF} = \begin{bmatrix} 0.757641 & 0.875928 & -8.91538\delta \\ -0.702611 & 0.468442 & 9.93225\delta \\ 0 & 0 & 1 \end{bmatrix}. \quad (39)$$

with a residual error of

$$T_{error} = T_{LSF} - T_{2,1} = \begin{bmatrix} 0.002332 & -0.000276 & -0.017520\delta \\ -0.000592 & -0.000504 & 0.005660\delta \\ 0 & 0 & 0 \end{bmatrix}. \quad (40)$$

The results of this least squares fit in terms of the fractional difference between the registered $S_{2,m,n}^{test}$ signal and the reference $S_{1,m,n}^{test}$ signal both with uncorrelated noise are shown in Figure 16.

The same noisy signals were registered using the fourth order Taylor expansion. The least squares fit converged in fourteen iterations yielding

$$T_{LSF} = \begin{bmatrix} 0.756448 & 0.876873 & -8.89075\delta \\ -0.702582 & 0.468279 & 9.93026\delta \\ 0 & 0 & 1 \end{bmatrix} \quad (41)$$

with a residual error of

$$T_{error} = T_{LSF} - T_{2,1} = \begin{bmatrix} 0.001139 & -0.000669 & 0.007110\delta \\ 0.000563 & -0.000667 & 0.003670\delta \\ 0 & 0 & 0 \end{bmatrix}. \quad (42)$$

The results of this least squares fit in terms of the fractional difference between the registered $S_{2,m,n}^{test}$ signal and the reference $S_{1,m,n}^{test}$ signal both with uncorrelated noise are shown in Figure 17.

The question arises with regard to the level of noise the least squares fit procedure can tolerate and still converge. In order for the least squares fit to converge to the signal values rather than quasi minimum associated with the noise on the signal, the magnitude of the noise must be small compared to the difference in the signal on average between adjacent pixels. This suggests that those pixels most effective in the least squares fit are associated with those parts of the signal with the greatest spatial gradients. For example, the maximum fraction difference in $S_{2,m,n}^{test}$ over one pixel distance is approximately 0.05. Our calculations indicate that the ability of this registration algorithm to register these particular signals diminishes significantly with fractional noise levels above about 0.01 as expected. The results in Figure 16 and Figure 17 show that clutter and jitter noise can be reduced down to the detector noise level providing the detector noise level is small compared to the fractional variation in the detector signal between adjacent pixels.

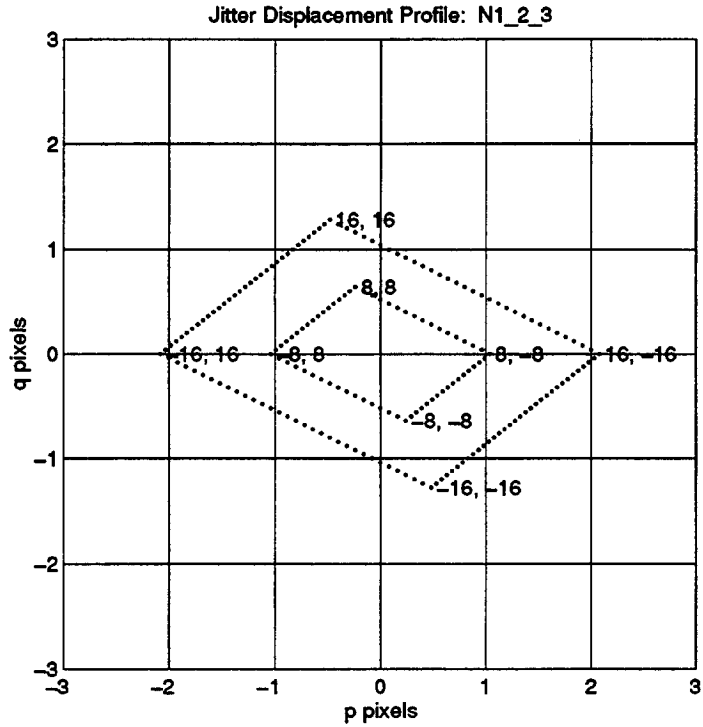


Figure 14 Plot of the displacement of the border pixels associated with each of the two subarrays centered on the detector array using the error matrix in Eq. (36). As the error matrix goes to zero, these points collapse to the origin.

fractional difference: M2_2_3

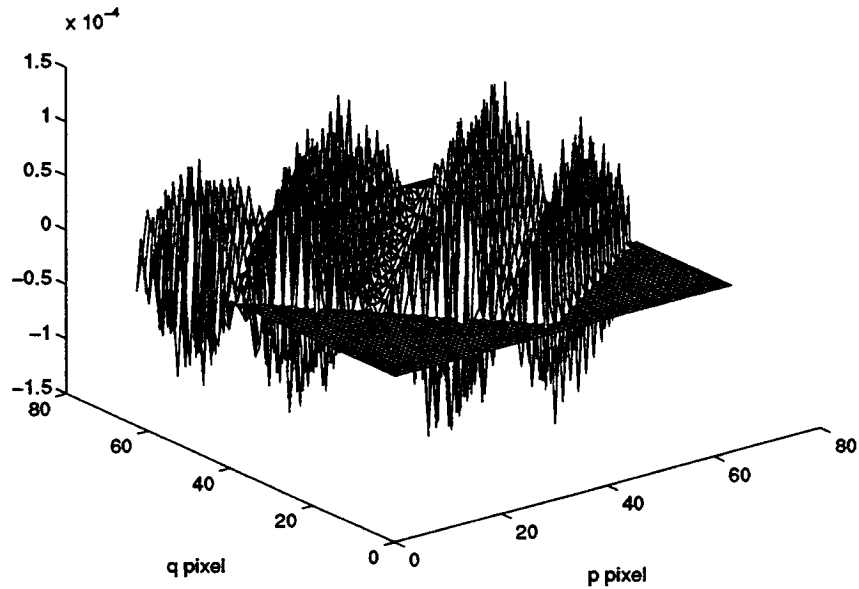


Figure 15 Plot of the fractional difference between the registered $S_{2,m,n}^{test}$ signal and the reference signal $S_{1,m,n}^{test}$ without noise using a second order Taylor expansion. The maximum fractional difference shown here is 1.2×10^{-4} .

fractional difference: M2_2_36

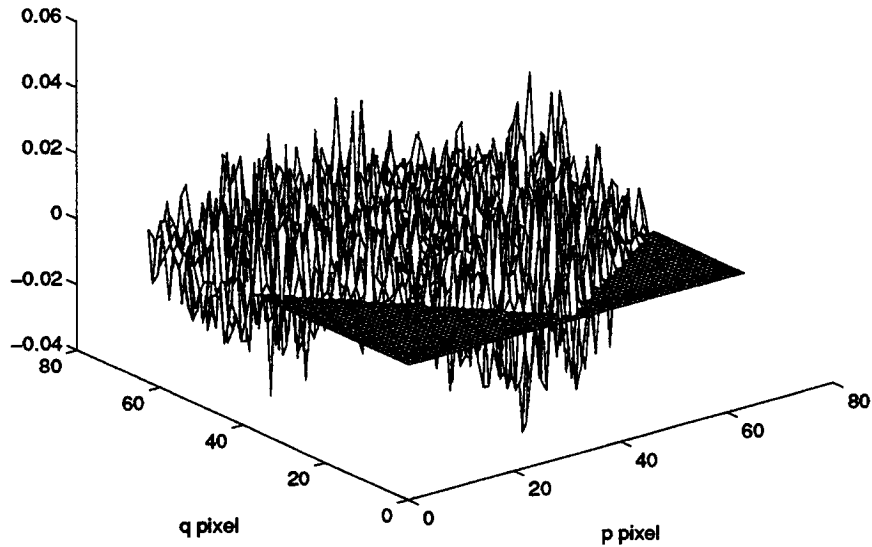


Figure 16 Plot of the fractional difference $fd_{k,m,n}$ between the registered $S_{2,m,n}^{test}$ signal using a second order taylor expansion and the reference signal $S_{1,m,n}^{test}$ with noise (0.02). The maximum value of $fd_{k,m,n}$ in this plot is 0.043.

fractional difference: M2_4_36

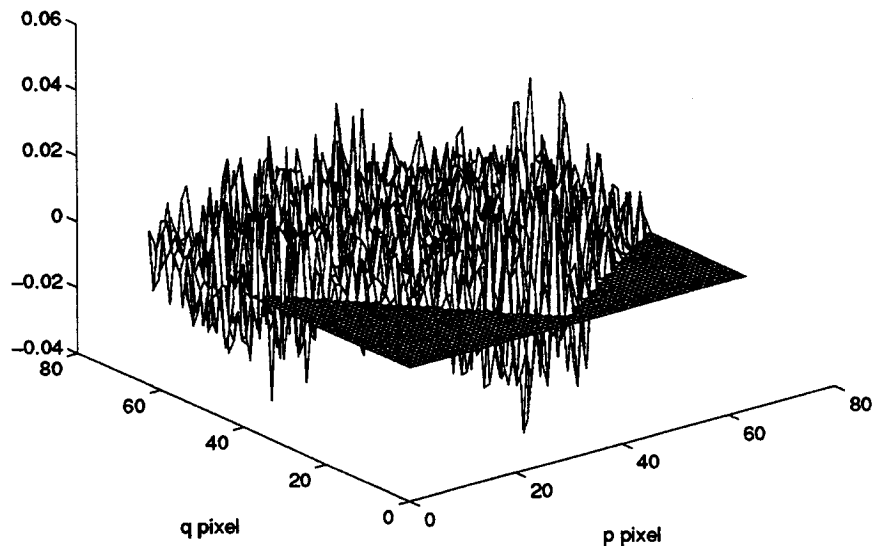


Figure 17 Plot of the fractional difference $fd_{k,m,n}$ between the registered $S_{2,m,n}^{test}$ using a fourth order taylor expansion and the reference signal $S_{1,m,n}^{test}$ with noise (0.02). The maximum value of $fd_{k,m,n}$ in this plot is 0.045.

7 Appendix: Integrals and Partial Derivatives

The function $H_k(X, Y)$ corresponds to

$$H_k(X, Y) = \sum_{r=0}^{\infty} \sum_{s=0}^r \frac{1}{s!(r-s)!} \frac{\partial^r G}{\partial x^s \partial y^{r-s}} \Big|_{k, m, n} (A_k X + B_k Y + C_k - x_m)^s (D_k X + E_k Y + F_k - y_n)^{r-s} \quad (43)$$

which is convergent in the neighborhood of the point ξ_k, ζ_k given by Eq. (17). The point ξ_k, ζ_k also corresponds to those respective values of X and Y in Eq. (43) for which

$$A_k X + B_k Y + C_k - x_m = 0 \quad (44)$$

$$D_k X + E_k Y + F_k - y_n = 0. \quad (45)$$

The registered signal associated with pixel M, N in the reference array at relative time k is $S_{k, M, N}^{reg}$ where

$$S_{k, M, N}^{reg} = \int_{(N-1)\delta}^{N\delta} \int_{(M-1)\delta}^{M\delta} H_k(X, Y) dX dY = \sum_{r=0}^{\infty} \sum_{s=0}^r \frac{1}{s!(r-s)!} \frac{\partial^r G}{\partial x^s \partial y^{r-s}} \Big|_{k, m, n} \Lambda_{r, s} \quad (46)$$

Consequently, it is necessary to evaluate integrals of the form

$$\Lambda_{r, s} = \int_{(N-1)\delta}^{N\delta} \int_{(M-1)\delta}^{M\delta} (A_k X + B_k Y + \alpha_m)^s (D_k X + E_k Y + \beta_n)^{r-s} dX dY \quad (47)$$

where

$$\alpha_m = C_k - x_m \quad (48)$$

and

$$\beta_n = F_k - y_n. \quad (49)$$

Keep in mind that m, n are the indices of the pixel in the detector array corresponding to signal $S_{k, m, n}$, and M, N are the indices of the pixel in the reference array to which the signal is to be registered [Eqs. (18) and (19)].

The $\Lambda_{r,s}$ integrals are represented here in terms of a row matrix \mathbf{K}_r and a column matrix $\mathbf{V}_{r,s}$ (the subscripts denote different matrices, not elements within the \mathbf{K}_r and $\mathbf{V}_{r,s}$ matrices) where

$$\Lambda_{r,s} = \mathbf{K}_r \mathbf{V}_{r,s}. \quad (50)$$

The time index k is dropped for the sake of notational simplicity from the transformation elements A_k, \dots, F_k in the following equations. Also the names $\mathbf{K}_r, \mathbf{V}_{r,s}, P_i(m), \mathbf{L}_j, \mathbf{S}_j, \mathbf{C}_j, \mathbf{Q}_j$ used to evaluate $\Lambda_{r,s}$ are local to this appendix.

For the zeroth order integral $\Lambda_{0,s}$,

$$\mathbf{K}_0 = \delta^2 \quad (51)$$

$$\mathbf{V}_{0,0}^T = 1. \quad (52)$$

For the first order integrals $\Lambda_{1,s}$,

$$\mathbf{K}_1 = \left[(P_2(M)P_1(N)) (P_1(M)P_2(N)) (\mathbf{K}_0) \right] \quad (53)$$

$$\mathbf{L}_1 = \left[(A) (B) \right] \quad (54)$$

$$\mathbf{L}_0 = \left[(D) (E) \right] \quad (55)$$

$$\mathbf{V}_{1,1}^T = \left[(\mathbf{L}_1) (\alpha_m) \right] \quad (56)$$

$$\mathbf{V}_{1,0}^T = \left[(\mathbf{L}_0) (\beta_n) \right] \quad (57)$$

where $\mathbf{V}_{r,s}^T$ is the transpose of the column matrix $\mathbf{V}_{r,s}$. By way of example

$$\begin{aligned} \Lambda_{1,0} &= \mathbf{K}_1 \mathbf{V}_{1,0} = \left[(P_2(M)P_1(N)) (P_1(M)P_2(N)) (\mathbf{K}_0) \right] \begin{bmatrix} D \\ E \\ \beta_n \end{bmatrix} \\ &= \delta P_2(M)D + \delta P_2(N)E + \delta^2 \beta_n. \end{aligned} \quad (58)$$

For the second order integrals $\Lambda_{2,s}$,

$$\mathbf{K}_2 = \left[(P_3(M)P_1(N)) (P_2(M)P_2(N)) (P_1(M)P_3(N)) (\mathbf{K}_1) \right] \quad (59)$$

$$\mathbf{S}_2 = \left[(A^2) (2AB) (B^2) \right] \quad (60)$$

$$\mathbf{S}_1 = \left[(AD) (AE + BD) (BE) \right] \quad (61)$$

$$\mathbf{S}_0 = \left[(D^2) (2DE) (E^2) \right] \quad (62)$$

$$\mathbf{V}_{2,2}^T = \left[(\mathbf{S}_2) (2\alpha_m \mathbf{L}_1) (\alpha_m^2) \right] \quad (63)$$

$$\mathbf{V}_{2,1}^T = \left[(\mathbf{S}_1) (\alpha_m \mathbf{L}_0 + \beta_n \mathbf{L}_1) (\alpha_m \beta_n) \right] \quad (64)$$

$$\mathbf{V}_{2,0}^T = \left[(\mathbf{S}_0) (2\beta_n \mathbf{L}_0) (\beta_n^2) \right] \quad (65)$$

For the third order integrals $\Lambda_{3,s}$

$$\mathbf{K}_3 = \left[\begin{array}{l} (P_4(M)P_1(N)) (P_3(M)P_2(N)) (P_2(M)P_3(N)) \\ (P_1(M)P_4(N)) (\mathbf{K}_2) \end{array} \right] \quad (66)$$

$$\mathbf{C}_3 = \left[(A^3) (3A^2B) (3AB^2) (B^3) \right] \quad (67)$$

$$\mathbf{C}_2 = \left[(A^2D) (2ABD + A^2E) (2ABE + B^2D) (B^2E) \right] \quad (68)$$

$$\mathbf{C}_1 = \left[(AD^2) (2ADE + BD^2) (2BDE + AE^2) (BE^2) \right] \quad (69)$$

$$\mathbf{C}_0 = \left[(D^3) (3D^2E) (3DE^2) (E^3) \right] \quad (70)$$

$$\mathbf{V}_{3,3}^T = \left[(\mathbf{C}_3) (3\alpha_m \mathbf{S}_2) (3\alpha_m^2 \mathbf{L}_1) (\alpha_m^3) \right] \quad (71)$$

$$\mathbf{V}_{3,2}^T = \left[(\mathbf{C}_2) (\beta_n \mathbf{S}_2 + 2\alpha_m \mathbf{S}_1) (\alpha_m^2 \mathbf{L}_0 + 2\alpha_m \beta_n \mathbf{L}_1) (\alpha_m^2 \beta_n) \right] \quad (72)$$

$$\mathbf{V}_{3,1}^T = \left[(\mathbf{C}_1) (2\beta_n \mathbf{S}_1 + \alpha_m \mathbf{S}_0) (\beta_n^2 \mathbf{L}_1 + 2\alpha_m \beta_n \mathbf{L}_0) (\alpha_m \beta_n^2) \right] \quad (73)$$

$$\mathbf{V}_{3,0}^T = \left[(\mathbf{C}_0) (3\beta_n \mathbf{S}_0) (3\beta_n^2 \mathbf{L}_0) (\beta_n^3) \right] \quad (74)$$

For the fourth order integrals $\Lambda_{4,s}$

$$\mathbf{K}_4 = \left[\begin{array}{l} (P_5(M)P_1(N)) (P_4(M)P_2(N)) (P_3(M)P_3(N)) \\ (P_2(M)P_4(N)) (P_1(M)P_5(N)) (\mathbf{K}_3) \end{array} \right] \quad (75)$$

$$\mathbf{Q}_4 = \begin{bmatrix} (A^4) & (4A^3B) & 6A^2B^2 & 4AB^3 & B^4 \end{bmatrix} \quad (76)$$

$$\mathbf{Q}_3 = \begin{bmatrix} [(A^3D)(A^2(AE + 3BD))(3AB(AE + BD)) \\ (B^2(3AE + BD)) (B^3E) \end{bmatrix} \quad (77)$$

$$\mathbf{Q}_2 = \begin{bmatrix} (A^2D^2) & (2AD(AE + BD)) & (A^2E^2 + B^2D^2 + 4ABDE) \\ (2BE(BD + AE)) & (B^2E^2) \end{bmatrix} \quad (78)$$

$$\mathbf{Q}_1 = \begin{bmatrix} (AD^3) & (D^2(3AE + BD)) & (3DE(BD + AE)) \\ (E^2(AE + 3BD)) & (BE^3) \end{bmatrix} \quad (79)$$

$$\mathbf{Q}_0 = \begin{bmatrix} (D^4) & (4D^3E) & (6D^2E^2) & (4DE^3) & (E^4) \end{bmatrix} \quad (80)$$

$$\mathbf{V}_{4,4}^T = \begin{bmatrix} (\mathbf{Q}_4) & (4\alpha_m \mathbf{C}_3) & (6\alpha_m^2 \mathbf{S}_2) & (4\alpha_m^3 \mathbf{L}_1) & (\alpha_m^4) \end{bmatrix} \quad (81)$$

$$\mathbf{V}_{4,3}^T = \begin{bmatrix} (\mathbf{Q}_3) & (\beta_n \mathbf{C}_3 + 3\alpha_m \mathbf{C}_2) & (3(\alpha_m \beta_n \mathbf{S}_2 + \alpha_m^2 \mathbf{S}_1)) \\ (3\alpha_m^2 \beta_n \mathbf{L}_1 + \alpha_m^3 \mathbf{L}_0) & (\alpha_m^3 \beta_n) \end{bmatrix} \quad (82)$$

$$\mathbf{V}_{4,2}^T = \begin{bmatrix} (\mathbf{Q}_2) & (2(\beta_n \mathbf{C}_2 + \alpha_m \mathbf{C}_1)) & (\beta_n^2 \mathbf{S}_2 + \alpha_m^2 \mathbf{S}_0 + 4\alpha_m \beta_n \mathbf{S}_1) \\ (2(\alpha_m^2 \beta_n \mathbf{L}_0 + \alpha_m \beta_n^2 \mathbf{L}_1)) & (\alpha_m^2 \beta_n^2) \end{bmatrix} \quad (83)$$

$$\mathbf{V}_{4,1}^T = \begin{bmatrix} (\mathbf{Q}_1) & (\alpha_m \mathbf{C}_0 + 3\beta_n \mathbf{C}_1) & (3(\alpha_m \beta_n \mathbf{S}_0 + \beta_n^2 \mathbf{S}_1)) \\ (3\alpha_m \beta_n^2 \mathbf{L}_0 + \beta_n^3 \mathbf{L}_1) & (\alpha_m \beta_n^3) \end{bmatrix} \quad (84)$$

$$\mathbf{V}_{4,0}^T = \begin{bmatrix} (\mathbf{Q}_0) & (4\beta_n \mathbf{C}_0) & (6\beta_n^2 \mathbf{S}_0) & (4\beta_n^3 \mathbf{L}_0) & (\beta_n^4) \end{bmatrix} \quad (85)$$

Note that the \mathbf{L} , \mathbf{S} , \mathbf{C} , \mathbf{Q} matrices are dependent upon only the transformation elements and therefore need be calculated only before each least squares iteration. The partial derivatives of the \mathbf{L} , \mathbf{S} , \mathbf{C} , \mathbf{Q} matrices with respect to A_k, \dots, F_k , which are required for the least squares fit procedure, are a simple function of the preceding \mathbf{L} , \mathbf{S} , \mathbf{C} , \mathbf{Q} matrix (for example, the partial derivatives of the \mathbf{S} matrix are a simple function of the \mathbf{L} matrices, etc.). The elements within the \mathbf{K} matrices need only be evaluated once, and the \mathbf{V} matrices need to be evaluated for each pixel in each least

squares fit iteration. The P_j parameters, which make up the \mathbf{K} matrices, are defined as

$$P_i(m) = \int_{(m-1)\delta}^{m\delta} \eta^{(i-1)} d\eta \quad (86)$$

so that

$$P_1(m) = \delta \quad (87)$$

$$P_2(m) = \frac{2m-1}{2} \cdot \delta^2 \quad (88)$$

$$P_3(m) = \frac{3m^2-3m+1}{3} \cdot \delta^3 \quad (89)$$

$$P_4(m) = \frac{4m^3-6m^2+4m-1}{4} \cdot \delta^4 \quad (90)$$

$$P_5(m) = \frac{5m^4-10m^3+10m^2-5m+1}{5} \cdot \delta^5 \quad (91)$$

where m is either a row or column pixel index in Eqs. (86) - (91) that ranges from $(-N_{pixels}/2) + 1$ to $N_{pixels}/2$. N_{pixels} is the total number of pixel rows or columns and must be even. The origin of the integration variable η in Eq. (86) is at the center of the array detector.

The least squares fit procedure requires an evaluation of the partial derivative of $S_{k,M,N}^{reg}$ with respect to each of the six transformation elements A_k, \dots, F_k where

$$\frac{\partial S_{k,M,N}^{reg}}{\partial \chi_j} = \sum_{r=0}^{\tau} \sum_{s=0}^r \frac{1}{s!(r-s)!} \frac{\partial^r G}{\partial x^s \partial y^{r-s}} \Big|_{k,m,n} \mathbf{K}_r \frac{\partial \mathbf{V}_{r,s}}{\partial \chi_j} \quad (92)$$

χ_j corresponds to the j th element in the sequence A_k, \dots, F_k . The partial derivatives of the $\mathbf{V}_{r,s}^T$ with respect to the χ_j are straight forward to derive. Also, certain symmetries exist among the partials themselves within each r manifold which can be utilized to alleviate the computational costs.

Within the software program, the correctness of the analytical partial derivatives $\frac{\partial \Lambda_{r,s}}{\partial \chi_j}$ should be verified at least once by a computational comparison with the numerical finite difference calculations of $\Lambda_{r,s}$ with respect to each transformation element; however, these finite differences should not be employed in place of the analytical partial derivatives.

This registration algorithm is the basis for two MATLAB codes [10]: one is based on an algebraic formulation and the other is based on the matrix formulation presented here. Although

the matrix formulation is more elegant, it is computationally more expensive as indicated in Table 2. Our MATLAB codes have been converted to C code by Scott Strong. Even though this algorithm is computational intensive, a least squares fit using every tenth pixel and registration of a 256×256 array detector takes approximately five seconds on a Silicon Graphics Onyx (R4000) workstation for a second order Taylor expansion.

Table 2: Relative MATLAB Computational Costs.

	Algebraic Formulation	Matrix Formulation
2nd Order Taylor Expansion	Number Flops: 211 Time (ms): 23	Number Flops: 561 Time (ms): 22
4th Order Taylor Expansion	Number Flops: 1134 Time (ms): 40	Number Flops: 4022 Time (ms): 68

8 Acknowledgments

This work has benefitted from discussions with Merle Benson, Karen Jefferson, John Rowe, Ron Schmidt, Scott Strong, and Richard Wickstrom of Sandia. This work was performed at Sandia National Laboratories and supported by the U.S. Department of Energy under Contract No. DE-AC04-94AL85000.

THIS PAGE LEFT INTENTIONALLY BLANK.

9 References

1. In anticipation of employing this algorithm within a system, it is advisable to verify its applicability by means of comprehensive simulation test.
2. L. G. Brown, "A Survey of Image Registration Techniques", *ACM Computing Surveys*, **24**(4), 325 - 376 (1992).
3. Q. Tian and M. N. Huhns, "Algorithms for Subpixel Registration", *Computer Vision, Graphics, and Image Processing*, **35**, 220 - 233 (1986).
4. A. Goshtasby, G. C. Stockman, and C. V. Page, "A Region-Based Approach to Digital Image Registration with Subpixel Accuracy", *IEEE Transactions on Geoscience and Remote Sensing*, **GE-24**(3), 390 - 399 (1986).
5. H. Li, B. S. Manjunath, and S. K. Mitra, "A Contour-Based Approach to Multisensor Image Registration", *IEEE Transactions on Image Processing*, **4**(3), 320 - 334 (1995).
6. K. Zikan, "Least Squares Image Registration", *ORSA Journal on Computing*, **3**(2), 169 (1991).
7. J. Flusser and T. Suk, "Pattern Recognition by Affine Moment Invariants", *Pattern Recognition* **26**(1), 167 - 174 (1993).
8. This argument is of course independent of pixel shape; however, the mathematics for pixels that are non-rectangular becomes more complex.
9. The coordinates of each vertex in Figure 1 can be transformed to the reference plane.
10. MATLAB (copyrighted by The MathWorks, Inc.) is a technical computing and graphical display environment.

THIS PAGE LEFT INTENTIONALLY BLANK.

Distribution

Sandia National Laboratories

1	MS 0987	R. D. Wickstrom, 2611
1	MS 0980	C. A. Boye, 5705
1	MS 0967	N. K. Blocker, 5706
1	MS 0980	K. R. Lanes, 5711
1	MS 0972	A. J. Medina, 5722
1	MS 0972	D. A. Dixon, 5722
1	MS 0972	R. R. Kay, 5722
1	MS 0980	P. J. Green, 5725
1	MS 0980	S. M. Gentry, 5725
1	MS 0980	K. J. Jefferson, 5725
1	MS 0980	L. N. Kmetyk, 5725
1	MS 0980	R. L. Schmidt, 5725
1	MS 0449	M. J. Benson, 6511
1	MS 0977	W. R. Cook, 6524
5	MS 0977	K. L. Brower, 6524
1	MS 0977	R. S. Longenbaugh, 6524
4	MS 1138	J. C. Rowe, 6531
1	MS 1138	D. S. Strong, 6531
1	MS 9018	Central Technical Files, 8940-2
5	MS 0899	Technical Library, 4414
2	MS 0619	Review and Approval Desk, 12690 for DOE/OST I

THIS PAGE LEFT INTENTIONALLY BLANK.